Journal of Biomedical Optics

BiomedicalOptics.SPIEDigitalLibrary.org

Depth-dependent autofluorescence photobleaching using 325, 473, 633, and 785 nm of porcine ear skin *ex vivo*

Johannes Schleusener
Jürgen Lademann
Maxim E. Darvin

SPIE.

Johannes Schleusener, Jürgen Lademann, Maxim E. Darvin, "Depth-dependent autofluorescence photobleaching using 325, 473, 633, and 785 nm of porcine ear skin *ex vivo*," *J. Biomed. Opt.* **22**(9), 091503 (2017), doi: 10.1117/1.JBO.22.9.091503.

Depth-dependent autofluorescence photobleaching using 325, 473, 633, and 785 nm of porcine ear skin *ex vivo*

Johannes Schleusener,* Jürgen Lademann, and Maxim E. Darvin
Charité—Universitätsmedizin Berlin, Center of Experimental and Applied Cutaneous Physiology, Department of Dermatology, Venerology and Allergology, Charitéplatz 1, 10117 Berlin, Germany

Abstract. Autofluorescence photobleaching describes the decrease of fluorescence intensity of endogenous fluorophores in biological tissue upon light irradiation. The origin of autofluorescence photobleaching is not fully understood. In the skin, the spatial distribution of various endogenous fluorophores varies within the skin layers. Most endogenous fluorophores are excited in the ultraviolet and short visible wavelength range, and only a few, such as porphyrins (red) and melanin (near-infrared), are excited at longer wavelengths. The excitation wavelength- and depth-dependent irradiation of skin will therefore excite different fluorophores, which will likely influence the photobleaching characteristics. The autofluorescence photobleaching of porcine ear skin has been measured *ex vivo* using 325, 473, 633, and 785 nm excitation at different skin depths from the surface to the dermis at 150 μm. Confocal Raman microscopes were used to achieve sufficient spatial resolution of the measurements. The autofluorescence area under the curve was measured for 21 consecutive acquisitions of 15 s. In all cases, the photobleaching follows a two-exponential decay function approximated by nonlinear regression. The results show that photobleaching can be applied to improve the signal-to-noise ratio in Raman spectroscopy for all of the applied excitation wavelengths and skin depths.
[DOI: 10.1117/1.JBO.22.9.091503]

Keywords: dermatology; confocal microscopy; Raman spectroscopy; fluorescence spectroscopy; stratum corneum; epidermis; dermis.

Paper 160629SSR received Sep. 9, 2016; accepted for publication Nov. 15, 2016; published online Jan. 5, 2017.

1 Introduction

The decrease of fluorescence intensity upon extended irradiation of biological tissue is referred to as the fluorescence photobleaching effect. Fluorescence photobleaching of exogenous fluorophores is widely used to determine the efficiency of photosensitizers, such as protoporphyrin IX, in photodynamic therapy.[1–4] The photobleaching of endogenous fluorophores of the skin can be utilized for different applications. In Raman spectroscopy, a fluorescent component is usually unwanted because a large background component complicates the analysis of Raman bands and can introduce artifacts during data analysis. In this case, fluorescence photobleaching can be exploited to decrease an autofluorescence component of the acquired spectra[5,6] because the Raman intensities do not bleach. Therefore, photobleaching by preirradiating the skin can be a useful method to improve the signal-to-noise ratio (SNR) of Raman spectra.[7] Darvin et al.[8] decreased the background of resonance Raman spectra by a factor 1.4 *in vivo*, and consequently the SNR could be improved by a factor of 1.2. Using photobleaching to preirradiate samples for Raman spectroscopy can allow longer acquisition times without risking saturation of the detector. A possible application for skin tumor diagnosis *in vivo* has been suggested by Lihachev et al.,[9] who found increased photobleaching rates in skin tumor lesions compared to normal skin in autofluorescence imaging at 405 nm excitation. A notable advantage of this method is the cost-effective application using merely a video camera instead of sophisticated spectroscopic instrumentation.[9–11]

Several decay models explaining the photobleaching dynamics have been described, ranging from one-[12,13] to three-exponential decay functions.[14] In most publications, the autofluorescence photobleaching was described by a two-exponential decay function[7,8,10,11,13,15–17]

$$I(t) = a \times e^{-\frac{t}{\tau_1}} + b \times e^{-\frac{t}{\tau_2}} + A. \quad (1)$$

Spigulis et al.[10] assumed that each skin surface chromophore has its dedicated autofluorescence bleaching rate in an *in vivo* study, while Zeng et al.[16,17] suggested that the fast decrease term (τ_1) corresponded to photobleaching effects within the stratum corneum (SC), while the slow decrease term (τ_2) was due to dermal effects in *in vivo* investigations.

In contrast to this interpretation, Berglund[18] claimed that the decay is truly nonexponential and that an exponential decay can solely be described by the spatially varying power density within the laser profile. Since higher intensity entails faster fluorescence decay,[4] the varying power density can introduce exponential decay rates. The simulations for this study were based on surface-immobilized fluorescent single molecules.

The origin of photobleaching is yet widely unknown. Fluorescence decay has been described to be due to the intersystem crossing of fluorophore molecules from a singlet to a

*Address all correspondence to: Johannes Schleusener, E-mail:johannes.schleusener@charite.de

1083-3668/2017/$25.00 © 2017 SPIE

triplet excited state. The rate at which the excited triplet state returns to the ground state is very low, entailing reduced fluorescence intensity.[19] This process is potentially reversible. A recovery of the autofluorescence from the skin in the range of 3 to 6 days after irradiation has been observed in several studies, which suggest photochemical effects of the endogenous fluorophores. These studies were performed *in vivo*[4,17] or were assumed to be performed *in vivo*.[3] Photobleaching has also been suggested to be due to the permanent photodecomposition of fluorophores.[19] Based on this assumption, fluorescence recovery after photobleaching (FRAP) has been used for analytical purposes, utilizing the diffusion of unbleached fluorophores into the bleached measurement volume.[20,21] The diffusion of unbleached fluorophores into the excited measurement volume could also be an explanation for fluorescence recovery in skin *in vivo*.

In addition to the nonfluorescing components, such as carotenoids,[8] the skin contains several endogenous fluorophores, such as reduced nicotinamide adenine dinucleotide, reduced nicotinamide adenine dinucleotide phosphate, structural proteins (collagen and elastin), aromatic aminoacids (tryptophan and tyrosine), porphyrins, oxidized flavin adenine dinucleotide (FAD), desmosine, lipofuscin, phospholipids, and keratin.[6,14,22–27] Most of these endogenous fluorophores are excited in the ultraviolet (UV) or short visible wavelength range.[28–30] Elastin, collagen, FAD, and keratin are excited in the blue wavelength region.[26,28] The autofluorescence of porphyrins and possibly flavins is excited by red and near-infrared (NIR) light.[4,28,31] Melanin does not fluoresce by UV and VIS excitation but is excited in the NIR range,[31,32] leading to increased autofluorescence intensities in pigmented skin lesions at 785 nm excitation.[33] Elastin, collagen, and lipids were also suggested to have a fluorescence contribution excited in the NIR.[7] The fluorophore concentration might also change upon irradiation. *In vivo* measurements of diffuse reflectance spectroscopy showed increased skin hemoglobin content after 405, 473, and 532 nm irradiance on the skin.[34]

The photobleaching dynamics is dependent on several factors. Fluorescein dissolved in poly(vinyl alcohol) has shown increased photobleaching at temperatures above the glass transition temperature T_g of the polymer host,[35] also temperature-dependent diffusion rates using FRAP were observed.[36] Several groups have investigated the skin fluorescence dependent on excitation wavelength, mostly in the UV and short visible wavelength range *in vivo*.[37] Lesins et al.[38] used different combinations of lasers for irradiation and preirradiation (405, 473, and 532 nm) and found faster autofluorescence photobleaching rates for shorter wavelengths *in vivo*.

In addition to the excitation of different fluorophores, the excitation wavelength also affects the penetration depth. The largest penetration into the skin occurs in the 600 to 1000 nm range, where light absorption and scattering are low.[26]

The distribution of the endogenous fluorophores in the skin varies in the different skin layers, and the fluorophore concentration in the upper dermis has been found to differ from that of the lower dermis *in vivo*.[37] The dermis is mostly constituted of collagen and elastin fibers;[23,39] collagen makes up 75% of its dry weight. The collagen content in the reticular dermis is especially high.[40] The viable epidermis, especially the SC, contain mostly keratin.[41–43] Melanin is produced in the melanocytes, which are located in the basal layer of the epidermis.[44,45] Zeng et al.[16,17] have used Monte Carlo simulation to model the contribution of autofluorescence of different skin layers for 442 nm excitation. The group determined 15% of the autofluorescence from the skin to result from the SC, while the remaining 85% of the fluorescence resulted from the dermis, where the majority of skin fluorophores are located. Differences of the autofluorescence in the upper and lower dermis were also found.[17] The viable epidermis without the SC was determined to be free of fluorescence due to the absence of fluorophors in this case, which was confirmed by measurements on 10 μm thin slices from the viable epidermis *ex vivo*.[17] Due to the excitation of different endogenous fluorophores, this behavior might change when exciting at different wavelengths. However, Wang et al.[46] found negligible fluorescence between the SC and the dermis using 785 nm excitation *ex vivo* on frozen skin and calculated the absorption- and scattering-based distortion of the intrinsic fluorescence spectra using Monte Carlo simulation. This is particularly interesting. Because of the melanin production in the melanocytes, located in the basal layer of the epidermis, it would appear reasonable to detect melanin-based fluorescence at NIR excitation from the epidermis. This could be an indication that epidermal melanin is not the major fluorophore in the skin, which is excited at 785 nm.

Zeng et al.[16] found the parameters a and b of the two-exponential decay [Eq. (1)] to increase, while parameters τ_1 and τ_2 decreased with higher excitation intensities *in vivo*. Debreczeny et al.[13] found the relation between the autofluorescence decay and the excitation intensity to be linear at 500 nm and nonlinear at 450 nm excitation wavelength. Further, the group found the autofluorescence decay to be independent of the skin type at 450 nm but significantly dependent on skin type at 500 nm excitation *in vivo*.[13] Similarly, Spigulis et al.[10] found the bleaching rates to be independent of the skin type *in vivo* for 405 nm excitation but dependent on skin type for 532 nm and concluded an influence of the epidermal melanin concentration. Lihachev and Spigulis[15] found differences of the slow decrease term (τ_2) for normal and pathological skin lesions at 405 and 532 nm excitation.

In this study, the autofluorescence photobleaching decay was measured at different depths, from the skin surface in the SC down to the dermis at 325, 473, 633, and 785 nm excitation on porcine ear skin samples *ex vivo*. Confocal Raman microscopes were used for a high spatial resolution of the different skin layers.

2 Materials and Methods

2.1 *Experimental Setup*

The experiments were performed using two confocal Raman microscopes on porcine ear skin *ex vivo* in the biological fingerprint region (400 to 1800 cm^{-1} for excitation at 473 and 785 nm and 700 to 1800 cm^{-1} for excitation at 325 and 633 nm). For the excitation at 325, 473, and 633 nm, a LabRAM HR Evolution (HORIBA Jobin Yvon, Longjumeau Cedex, France) with a comprised BX41 microscope (Olympus, Tokyo, Japan) was used. For the excitation at 473 and 633 nm, a 600-g/mm grating, an MPlan N VIS2 50× objective (Olympus, Tokyo, Japan), and an ∅100-μm pinhole were used. A 2400-g/mm grating, an LMU-40X-NUV objective (Thorlabs, Newton, New Jersey), and an ∅200-μm pinhole were used for excitation at 325 nm. Both gratings were blazed at 500 nm. A 325 nm IK3301 R-G He-Cd laser (Kimmon Koha Co., Ltd., Tokyo, Japan), a 473 nm Cobolt Blues 25-mW diode laser (Cobolt AB, Solna, Sweden), and a

633-nm HeNe laser (Melles Griot, Carlsbad, California) were used as excitation sources, delivering 8.1, 6.1, and 8.4 mW of optical power, respectively, to the sample surface. The spectral resolution was <4 cm^{-1}. Data acquisition was performed using the associated LabSpec 6.4 software. This device was described in detail elsewhere.[47]

For NIR excitation, a Model 3510 Skin Composition Analyzer (SCA) confocal Raman microscope (River Diagnostics B.V., Rotterdam, The Netherlands) suitable for *in vivo* and *ex vivo* measurements with a 50× oil objective and a 785 nm laser (Innovative Photonic Solutions, Monmouth Junction, New Jersey) was used. The spot size was 5 μm and an optical power of 22 mW on the skin surface was used. An axial resolution of < 5 μm, as well as a spectral resolution of 2 cm^{-1}, was achieved. This device was described in detail elsewhere.[48,49]

2.2 *Experiments*

The experiments were conducted *ex vivo* on unpigmented, untreated, not preirradiated porcine ears, serving as a skin model,[50] at a maximum of 3 days after slaughter. The hair was carefully removed from the skin without influence on the SC, and the samples were stored at 4°C before the measurements, which were performed at 22°C room temperature. Measurements were performed in 21 consecutive acquisitions of 15 s, resulting in a total experiment time of 315 s with continuous irradiation for every sample. A total of $n = 6$ measurements were taken at ≈0, 10, 15, 20, 50, 120, and 150 μm depths for every applied excitation wavelength. Depths 0 to 15 μm were assumed to be located within the SC,[43,45,51–54] depths 20 to 50 μm in the viable epidermis,[44,45,55] and depths 120 to 150 μm within the papillary dermis. Deviations of the measured depth in the skin due to varying refractive index in the different skin layers[41] were neglected.

The position of the skin surface was determined after the photobleaching experiment, by performing a z-scan of Raman measurements from 40 μm above to 40 μm below the visual focus plane in 2 μm increments, while maintaining the x- and y-positions of the sample. After baseline removal, the height of the 1654 cm^{-1} amide I Raman band was analyzed as a function of the z-position. For 325 nm excitation, this was done with the band around 1600 cm^{-1}. The skin surface was then defined to be the position with 50% of the maximum peak height.[56] For the measurements with the Model 3510 SCA, a similar procedure could be automatically performed using the nonrestricted multiple least squares fit method of the keratin profile using the "Skin Tools 2.0" software (River Diagnostics B.V., Rotterdam, The Netherlands), which was explained in detail elsewhere.[57]

2.3 *Data Analysis*

All data analysis was performed in MATLAB® R2016a (The MathWorks, Inc., Natick, Massachusetts). To analyze the fluorescence dynamics, the area under the curve (AUC) was calculated using trapezoidal numerical integration in the 400 to 700, 700 to 1100, 1100 to 1500, and 1500 to 1800 cm^{-1} ranges. This was done to examine a possible wavelength-dependent photobleaching effect. For analysis of the AUC, cosmic spikes were removed, using a seventh-order median filter. Due to reduced dispersion of the 600-g/mm grating at 633 nm and the 2400-g/mm grating at 325 nm excitation, the 400 to 700 cm^{-1} range was omitted in these cases. The autofluorescence intensity was normalized by dividing by the intensity of the initial acquisition at $t = 15$ s.

The autofluorescence decay was fitted to a double-exponential decay function [Eq. (1)] using nonlinear regression for every measurement. Peak heights for the 1003 cm^{-1} phenylalanine and urea, the 1452 cm^{-1} $\delta(CH_2)(CH_3)$, and the 1654 cm^{-1} amide I bands were analyzed by fitting a Gaussian function to the baseline removed spectra. For 325 nm excitation, this was done for the band around 1600 cm^{-1} due to the different spectral shape.

3 Results and Discussion

3.1 *Raw Spectra*

Figure 1 shows exemplarily the mean of $n = 6$ measurements for 10 μm depths in the skin for 325 (a), 473 (b), 633 (c), and 785 nm (d) at the consecutive acquisition times from 15 to 180 s. The total intensity of the fluorescence is highly dependent on the fluorophore concentration in the measured volume and varies strongly for repeating measurements, which becomes especially obvious for smaller measurement volumes, using confocal microscopy. However, the maximum fluorescence intensity of the mean of six measurements at 473 nm excitation is higher by a factor of ≈2 compared to the excitation at 633 nm, despite a 1.3 times smaller excitation power (6.1 mW for 473 nm and 8.4 mW for 633 mW). This would be in agreement with the expected loss of fluorescence at increased excitation wavelengths. The fluorescence intensity at 325 nm excitation is considerably reduced, compared to 473 and 633 nm, which can be explained by the wavelength-dependent absorption- and scattering-based intensity loss, entailing smaller penetration depths at UV excitation. The results for 785 nm [Fig. 1(d)] were acquired using different instrumentation at 22 mW. For a detailed analysis of the total fluorescence, a wavelength-dependent light throughput of the detecting optics, as well as the detector sensitivity, would have to be taken into account.[58] Because of scattering, absorption, and anisotropy propagation, the total intensity of the spectra decreases with increasing depth in the skin (data not shown). The Raman/fluorescence ratio clearly increases during the photobleaching process, which is in accordance with previously published data.[8]

In contrast to the fluorescence, the Raman intensities do not bleach over extended irradiation. To verify this expected behavior, the Raman peak heights for the 1003, 1452, and 1654 cm^{-1} bands were recorded during the 315 s irradiation. After baseline removal, no change in peak intensities could be observed. The spectral shape for 325 nm excitation [Fig. 1(a)] is clearly distinct from the visible and NIR excitation, which was previously also observed on cell measurements.[59] Only a band around 1600 cm^{-1} can be identified. The intensity of this band, however, does also not decrease during autofluorescence photobleaching.

3.2 *Autofluorescence Photobleaching*

Figure 2 shows the mean of the normalized autofluorescence decay for the measured depths at 325, 473, 633, and 785 nm excitation. Although the fluorescence intensity shown in Fig. 1 is wavenumber dependent, as evident by the skew of the spectra, especially for 325 and 473 nm excitation, a difference in the bleaching rate depending on the wavenumber range as

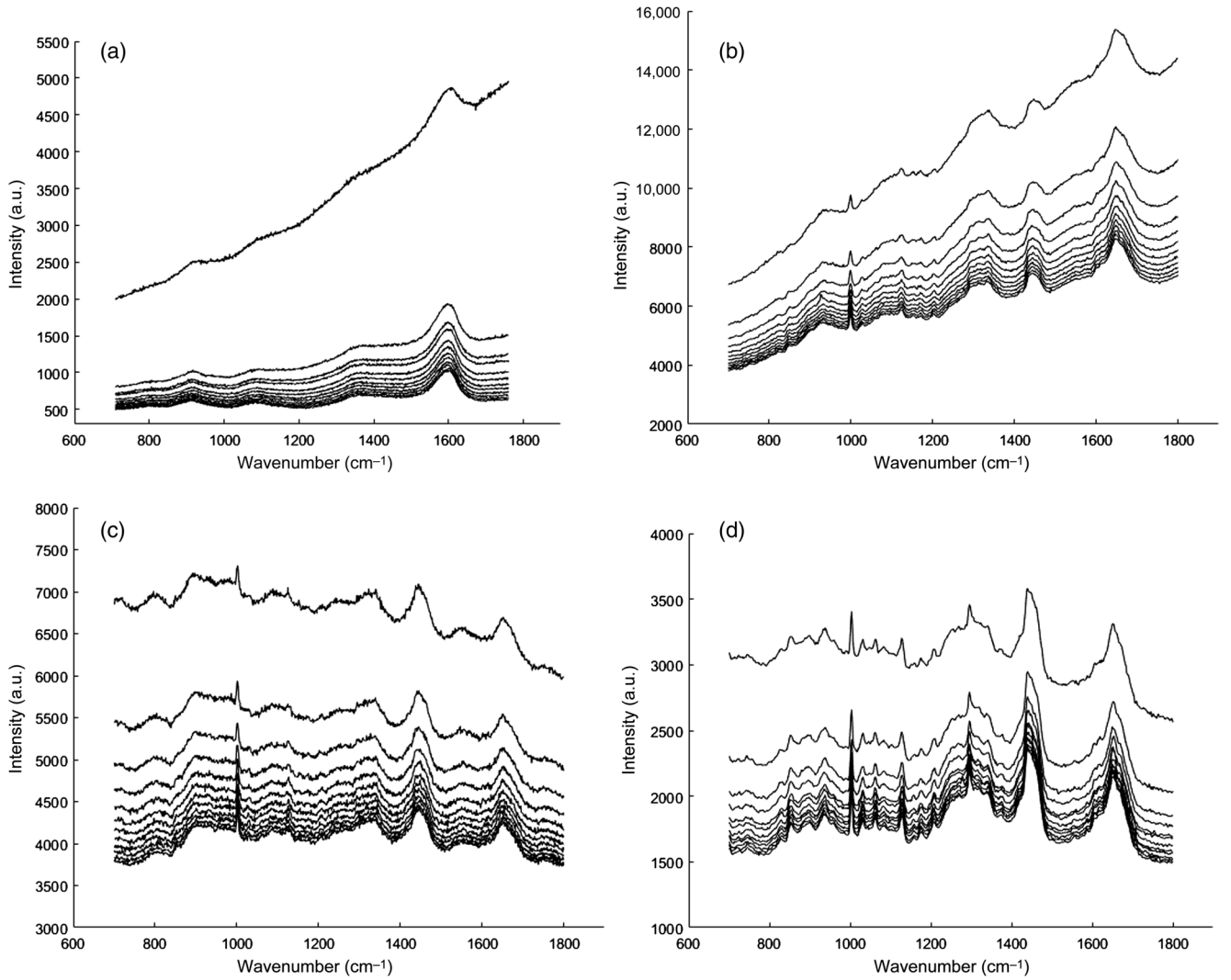

Fig. 1 Example for the photobleaching effect at (a) 325 nm (8.1 mW), (b) 473 nm (6.1 mW), (c) 633 nm (8.4 mW), and (d) 785 nm excitation (22.0 mW). The spectra show the mean of six measurements at 10 μm depths in the SC for 12 consecutive acquisitions of 15 s. The fluorescence intensity decreases with every acquisition.

defined in the data analysis section could not be found. Therefore, Fig. 2 only shows the photobleaching of the complete 700 to 1800 cm^{-1} range. The standard deviation 1 σ was $\leq$0.1 ($\leq$0.2 for 325 nm excitation at 0 μm depth in skin), but for clarity, error bars are omitted in the figures.

The results indicate that a nonlinear photobleaching occurs for all excitation wavelengths in all the measured skin depths. The largest decay occurs for 325 nm excitation, where the autofluorescence decreases from 18% to 29% of its initial intensity. For 473 nm excitation, the fluorescence intensity decreases from 39% to 54% of its initial value at all skin depths after 315 s irradiation. The decrease for 633 nm excitation is only slightly reduced from 36% to 60% of its initial intensity. Despite a >2.5 times higher excitation power at 785 nm, the autofluorescence decay is considerably smaller, as the fluorescence intensity decreases only from 50% to 80% of the initial value in this case. The initial fluorescence at 785 nm excitation is severely reduced compared to 325, 473, and 633 nm, and it is assumed that only few fluorophores in the skin are excited by NIR light.

Excitation at 325 nm has a considerably lower penetration depth, therefore, only depths in the SC are shown. The largest decay occurs at 10 μm depth, where the fluorescence intensity decreases to <20% after 315 s irradiation. Measurements below the SC cannot be reasonably performed at 325 nm excitation. Although a majority of endogenous fluorophores are excited in the UV wavelength range, the main effect of autofluorescence photobleaching in this case is likely related to keratin, which is the main skin component in the SC. For excitation at 473 nm and 633 nm, the largest decay occurs at 50 μm depth in the skin, which represents the stratum spinosum layer of the viable epidermis, with fluorescence intensity of 35% to 40% of the initial value after 315 s irradiation. The decay in the SC (0 and 10 μm) was the smallest in this case (50% to 60% of the initial value). For the 785 nm excitation, the largest decay occurs in the SC between 0 and 15 μm in the skin (50% to 55% of the initial value after irradiation) and considerably smaller bleaching in the dermis (120 to 150 μm), where the fluorescence intensity only dropped to 75% to 80% of the initial value after 315 s irradiation. The major fluorophore excited by 785 nm is assumed to

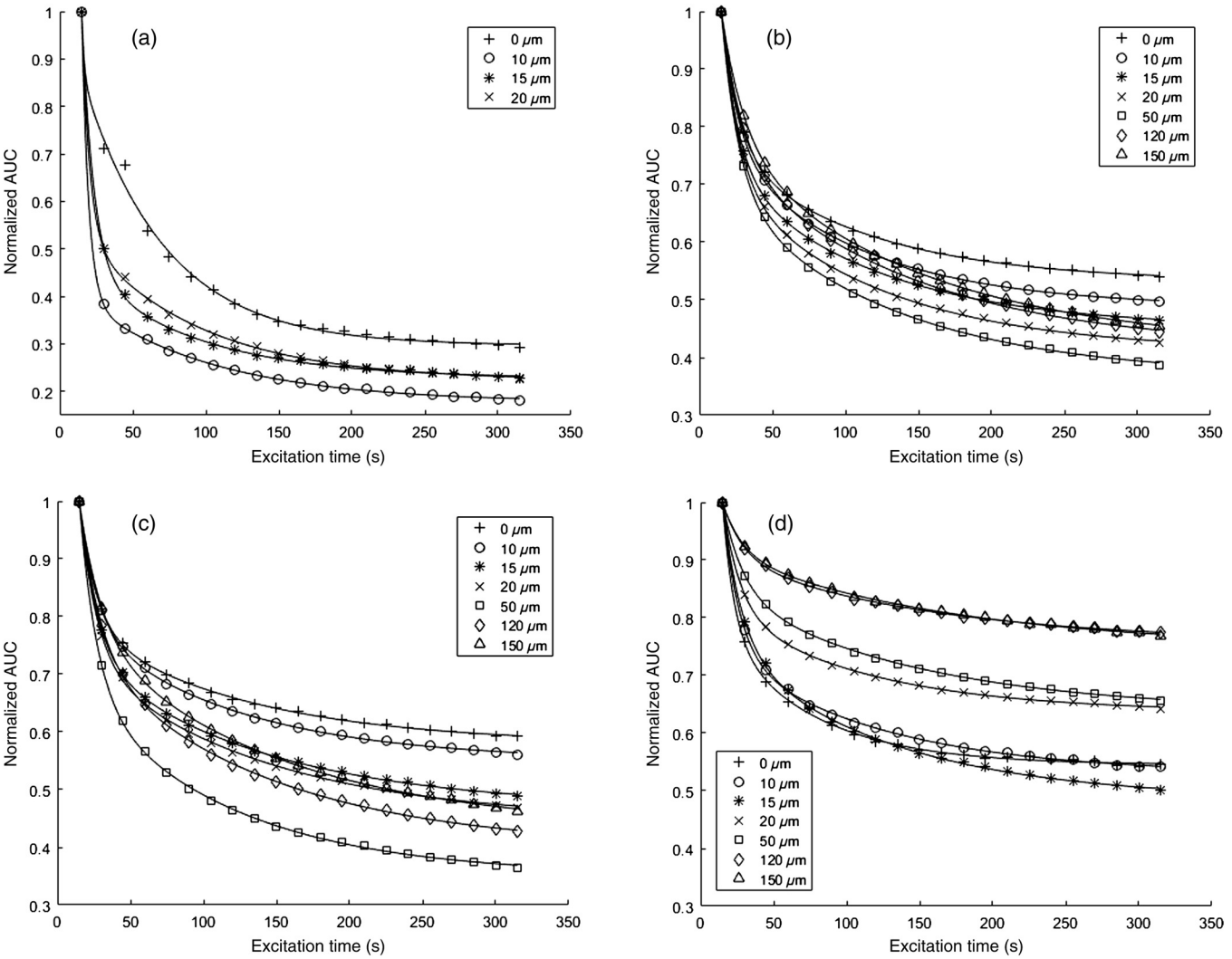

Fig. 2 Mean normalized decay of AUC for six repeative measurements in the 700 to 1800 cm^{-1} wavenumber range using (a) 325 (8.1 mW), (b) 473 (6.1 mW), (c) 633 (8.4 mW), and (d) 785 nm excitation (22.0 mW) at different depths in the skin.

be melanin, which is located mainly in the lower epidermis. These results indicate that the fluorescence photobleaching by 785 nm excitation mainly occurs for endogenous fluorophores located in the epidermis, which is likely melanin. These results disagree with the findings of Wang et al.,[46] who found only negligible fluorescence in the epidermis at 785 nm excitation. This needs to be further elucidated. The comparatively small photobleaching component in the dermis could possibly result from collagen and elastin,[7] which are also the main dermal components. However, collagen and elastin mainly fluoresce under blue excitation, which is likely the origin of the moderate photobleaching at 473 nm excitation below 100 μm in the skin. The relatively small amount of autofluorescence photobleaching in the SC (0 to 10 μm) at 473 nm excitation may result from keratin to a large extent, which is the major component of the SC.[41] Our results do not indicate autofluorescence free layers in the skin at either of the applied excitation wavelengths.

Using the confocal Raman microscope, a possible long-term drift of the laser focus position due to the drying of the sample may occur; hence, measurements to examine a possible recovery of the autofluorescence could not be performed. Zeng[17] noticed a fluorescence recovery *in vivo* after 6 days, while Stratonnikov et al.[4] examined a recovery after 3 to 5 days after *in vivo* laser irradiation. In the study by Lihachev et al.,[3] autofluorescence recovery to 80% of the initial value took <5 days. The origin of the fluorescence recovery is not fully understood. A possible explanation is the diffusion of unbleached fluorophores to the irradiated area, as explained for FRAP measurements.[19,20] In contradiction, the results by Zeng[17] indicated that this was not the explanation for the fluorescence recovery in their presented data; instead, a long-term photochemical reaction was suggested to be more probable than photo decomposition of the endogenous fluorophores. In the case of decomposition of the irradiated molecules, a decrease of the Raman signal would also be expected, which was not recognized in the presented data.

3.3 *Photobleaching Decay Parameters*

The two-exponential decay function was used for a nonlinear regression approximation of the autofluorescence decay. The offset parameter A in the decay function [Eq. (1)] is a measure of the baseline fluorescence intensity of the spectra that is not bleached. This parameter varies depending on the measured skin

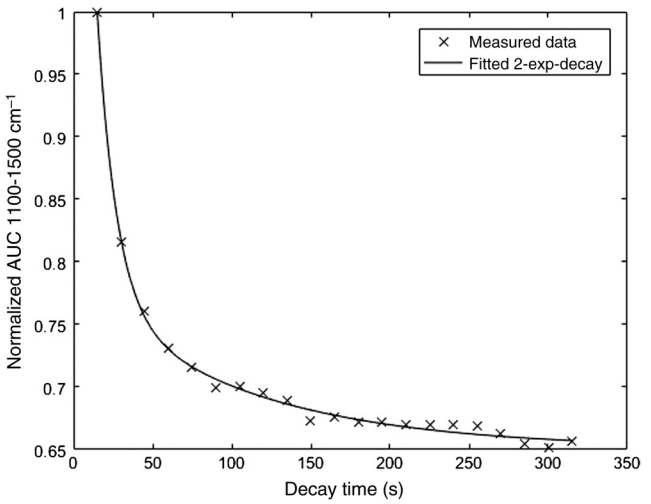

Fig. 3 Example for autofluorescence decay normalized AUC for 15 to 315 s 785 nm excitation. Measured in the SC (10 μm skin depth) in the 1100 to 1500 cm^{-1} wavenumber range. The data are fitted to a double-exponential decay function [Eq. (1)] by nonlinear regression (R-squared = 0.997). $\tau_1 = 12.262$, $\tau_2 = 103.081$, $a = 0.800$, $b = 0.131$, and $A = 0.651$.

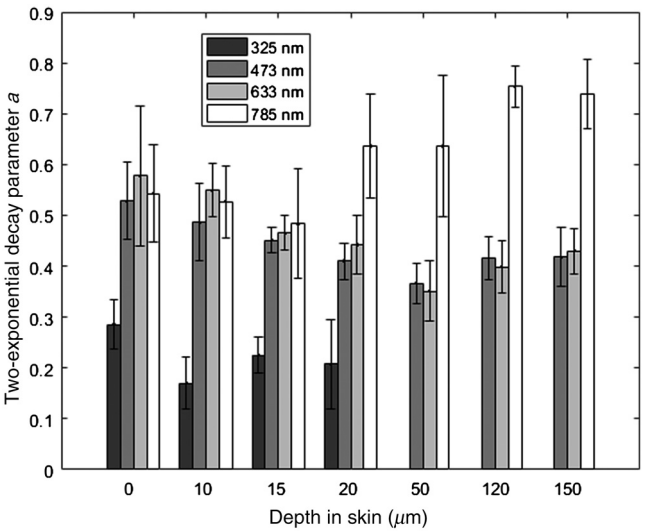

Fig. 4 Autofluorescence photobleaching decay parameter A of double-exponential decay function [Eq. (1)] using 325, 473, 633, and 785 nm excitation for different depths in the skin in the 700 to 1800 cm^{-1} wavenumber range. The mean of six measurements with error bars representing ±standard deviation 1 σ is shown.

position and, hence, the availability of fluorophores in the measured volume,[16] which is in agreement with other published data.[12] τ_1 and a describe a fast decrease component of the decay function while τ_2 and b describe a slow decrease component. The parameters τ_1 and τ_2 indicate the rate while parameters a and b indicate the fraction of the photobleaching decay for each of the components.[16] Figure 3 shows an example of the experimental decay data in the 1100 to 1500 cm^{-1} region for 785 nm excitation and the two-exponential decay function fitted by nonlinear regression (R-squared = 0.997).

The photobleaching could be described by the two-exponential decay function in all skin depths at all applied excitation wavelengths. Former suggestions that the two components of the decay function represent the photobleaching of the SC and the dermis, respectively,[16,17] could not be verified by our results because every measurement is limited to a single skin layer due to the use of confocal microscopy.

The differences in the amount of photobleaching, as discussed in Fig. 2, correlate to the offset parameter A, as shown in Fig. 4. A significant difference of the photobleaching depending on the detected wavenumber ranges (400 to 700, 700 to 1100, 1100 to 1500, and 1500 to 1800 cm^{-1}) could not be determined using one-way analysis of variance (ANOVA, $p > 0.25$) for either of the applied excitation wavelengths (data not shown). A reduced residual fluorescence that is not bleached during excitation can clearly be noticed for UV excitation. The largest photobleaching component at a depth of 50 μm, as explained in Fig. 2, is represented by the lowest parameter A for 473 and 633 nm excitation. For 785 nm excitation, the residual fluorescence is lowest in the SC and increases in the viable epidermis, especially in the papillary dermis.

These findings are not reflected in the bleaching rate parameters τ_1 and τ_2, which means that a large bleaching does not necessarily occur at a fast rate.

Figure 5 shows the decay parameters τ_1 and τ_2 for the 700 to 1800 cm^{-1} wavenumber range. No significant differences of the photobleaching rates depending on the detected wavenumber ranges were found (ANOVA, $p > 0.25$). In the case of influence of multiple fluorophores emitting with differing emission maxima, this could be an indication that the photobleaching rates for these fluorophores are equal. In the *in vivo* study by Zeng et al.,[16] using 442 nm excitation, only minor wavelength dependence of the fitting parameters was found.

For excitation at 473 and 633 nm, the parameter τ_1 is largest in the dermis (120 to 150 μm), representing a slower bleaching of the fast decay component (Fig. 5), while a moderate amount of photobleaching in the dermis can be seen in Fig. 2. For 785 nm excitation, the parameters τ_1 and τ_2 are reduced at the skin surface and in the SC, which represents a faster bleaching process. Large deviations can be seen for excitation at 325 nm. At 0 μm depth, τ_1 is 2.6 to 4.3 times larger compared to the deeper measurements, which reach to the bottom of the SC. However, the standard deviation is 137% of τ_1 in this case. In the case of UV excitation, a considerable dark spot on the skin sample and the formation of an air gap between the sample and the cover slide in the microscopic video image were noticed. It is likely that the skin surface position was not stable during the measurements at UV excitation, which could explain the large deviations. τ_2, which represents the slow bleaching component, generally increases with increasing depth in the skin. A possible explanation could be the depth-dependent intensity loss of the excitation.

Zeng[17] found *in vivo* that the fast and slow decay parameters τ_1 and τ_2 differed by an order of magnitude, which was confirmed by our results. Also in the *in vivo* study by Wang et al.[7] using 785 nm excitation, τ_1 and τ_2 differed by an order of magnitude. The ratio τ_1/τ_2 was between 0.08 and 0.12 in our results, except for excitation at 325 nm, where τ_1/τ_2 was 0.3 at 0 μm and 0.05 at 10 and 20 μm depth in the skin.

Figure 6 shows the two-exponential decay parameters a and b. Analog to τ_1 and τ_2 a one-way ANOVA showed no significant differences depending on the wavenumber ranges ($p > 0.25$); therefore, only the 700 to 1800 cm^{-1} range is shown. For clarity, the parameter a is not shown for 325 nm excitation; the value

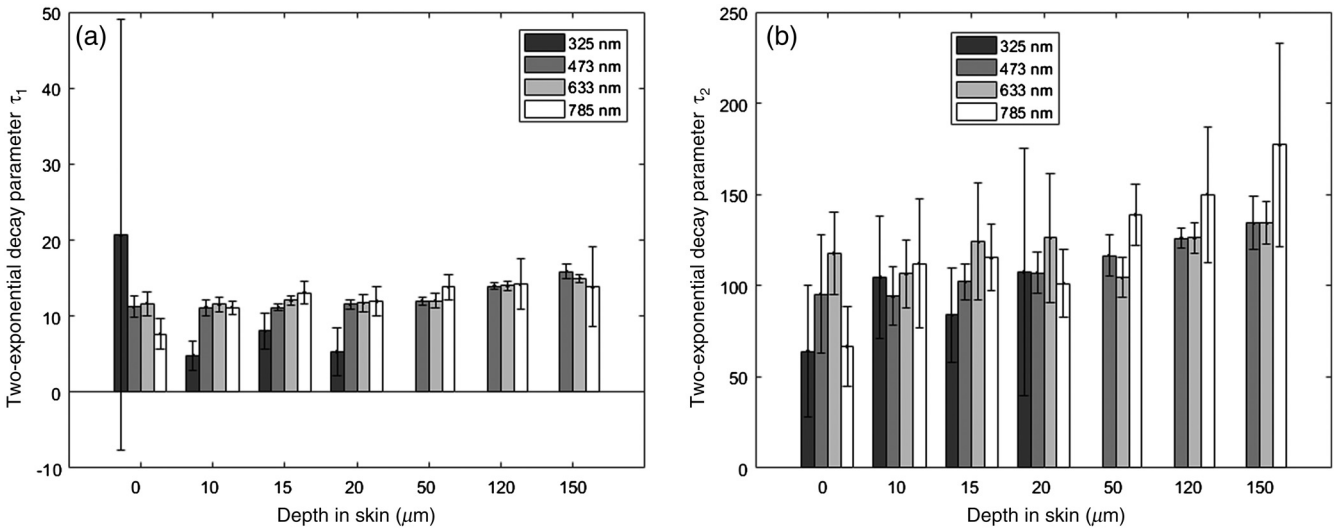

Fig. 5 Autofluorescence photobleaching decay parameters (a) τ_1 and (b) τ_2 of double-exponential decay function [Eq. (1)] using 325, 473, 633, and 785 nm excitation for different depths in the skin in the 700 to 1800 cm^{-1} wavenumber range. The mean of six measurements with error bars representing $\pm$standard deviation 1 σ is shown.

was increased by a factor of $\approx$4 for 15 μm and was 3 orders of magnitude larger for 0, 10, and 20 μm depth in the skin, with standard deviations 1 σ of up to 180% of a. The large deviations in the case of UV excitation could be explained by a possible movement of the skin surface during irradiation. Large deviations also occur for the b parameter for 325 nm excitation at 0 μm depth in the skin, which has a standard deviation 1 σ of 50%. For 473 and 633 nm excitation, an increase of a and b with increasing depth in the skin can be observed, with the exemption of a decrease of a in the papillary dermis. In reverse, a and b decrease with increasing depths in the skin for 785 nm excitation.

The b/a ratio for 473, 633, and 785 nm is between 0.3 and 0.4 for all depths in the skin, with the only exception of 0.2 for 785 nm at 0 μm depth, which can be explained by the increased a in this case. For 325 nm excitation, the b/a ratio is between 0.001 and 0.06, indicating a larger contribution of the fast decay component (parameter a is not shown for 325 nm for clarity).

A direct comparison of the photobleaching rates is challenging because they are dependent on the irradiation intensities. Linear and nonlinear relations between excitation intensity and fluorescence have been found, depending on the excitation wavelength.[13] The excitation intensity is in return dependent on the depth within the skin due to absorption- and scattering-based

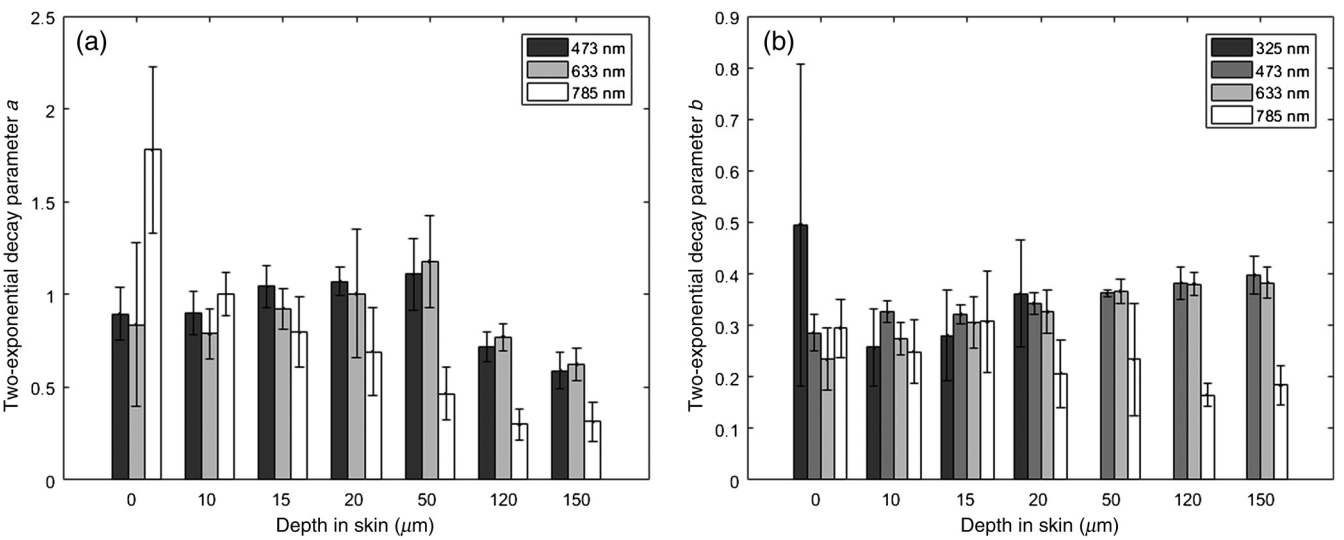

Fig. 6 Autofluorescence photobleaching decay parameters (a) a and (b) b of double-exponential decay function [Eq. (1)] using 325, 473, 633, and 785 nm excitation for different depths in the skin in the 700 to 1800 cm^{-1} wavenumber range. For clarity, parameter a is not shown for 325 nm. Compared to the other excitation wavelengths, the value was increased by a factor of $\approx$4 for 15 μm and was 3 orders of magnitude larger for 0, 10, and 20 μm. The mean of six measurements with error bars representing $\pm$standard deviation 1 σ is shown.

attenuation. Furthermore, the absorption and scattering in the skin are wavelength dependent, entailing a higher penetration depth at 785 nm than at the 473 and 633 nm visible excitation wavelengths and severely reduced penetration depth only at 325 nm. Further investigations are necessary to compensate the depth- and wavelength-dependent irradiation and autofluorescence intensities. One approach could be the fluorescence normalization based on the keratin contribution of the recorded Raman spectra,[58] as the keratin distribution within the SC is considered to be homogenous.[41,56] However, for deeper skin layers, the normalization is a very complicated task due to the inhomogeneous distribution of the fluorophors. Franzen et al.[60] developed an algorithm for compensated depth-dependent intensity loss that was based on measurements on a skin phantom incubated with known homogenous drug concentrations and obtained homogenous drug-based Raman intensities in the corrected depth profiles. Challenges for such approaches might arise for physiologic variations, such as varying thickness of skin layers depending on the body site.

4 Conclusion

The presented results show that the autofluorescence photobleaching of the skin at 325, 473, 633, and 785 nm excitation wavelength can be described by the two-exponential decay function for different depths in the skin from the skin surface to the papillary dermis (0 to 150 μm), or in the case of UV irradiation within the SC. The results do not indicate skin layers free of autofluorescence at the applied excitation wavelengths. A dependence of the determined autofluorescence photobleaching rates on the detected wavenumber range in the fingerprint region could not be found. An assignment of the major endogenous fluorophores responsible for the photobleaching has been attempted based on the known excitation wavelengths and location within the skin.

Autofluorescence photobleaching can be applied to improve the SNR for Raman spectroscopy by 473, 633, and 785 nm excitation. For 325 nm excitation, the Raman spectra are difficult to interpret, but a decrease of Raman intensity was not observed either. For this purpose, the parameters τ_1 and τ_2 of the two-exponential decay function can specify a useful time range for preirradiation.

The presented results are based on the normalized autofluorescence photobleaching referring to the initial fluorescence intensity after 15 s of excitation. To gain insight about the absolute autofluorescence originating from the different skin layers, further research is necessary, taking into account the absorption- and scattering-based signal decrease at increasing skin depths. The same tendencies are expected for *in vivo* skin measurements.

Disclosures

The authors report no conflicts of interest.

References

1. A. V. Ryabova, A. A. Stratonnikov, and V. B. Loshchenov, "Laser spectroscopy technique for estimating the efficiency of photosensitisers in biological media," *Quantum Electron.* **36**(6), 562–568 (2006).
2. A. Sharwani and F. A. Alharbi, "Monitoring of photobleaching in photodynamic therapy using fluorescence spectroscopy," *Gulf J. Oncol.* **1**(16), 79–83 (2014).
3. A. Lihachev et al., "Low power CW-laser signatures on human skin," *Quantum Electron.* **40**(12), 1077–1080 (2010).
4. A. A. Stratonnikov, V. S. Polikarpov, and V. B. Loschenov, "Photobleaching of endogenous fluorochroms in tissues in vivo during laser irradiation," *Proc. SPIE* **4241**, 13–24 (2001).
5. J. Kostamovaara et al., "Fluorescence suppression in Raman spectroscopy using a time-gated CMOS SPAD," *Opt. Express* **21**(25), 31632–31645 (2013).
6. M. E. Darvin et al., "Comparison of two methods for noninvasive determination of carotenoids in human and animal skin: Raman spectroscopy versus reflection spectroscopy," *J. Biophotonics* **5**(7), 550–558 (2012).
7. H. Wang et al., "Improving skin Raman spectral quality by fluorescence photobleaching," *Photodiagn. Photodyn. Ther.* **9**(4), 299–302 (2012).
8. M. E. Darvin, N. N. Brandt, and J. Lademann, "Photobleaching as a method of increasing the accuracy in measuring carotenoid concentration in human skin by Raman spectroscopy," *Opt. Spectrosc.* **109**(2), 205–210 (2010).
9. A. Lihachev et al., "Autofluorescence imaging of basal cell carcinoma by smartphone RGB camera," *J. Biomed. Opt.* **20**(12), 120502 (2015).
10. J. Spigulis, A. Lihachev, and R. Erts, "Imaging of laser-excited tissue autofluorescence bleaching rates," *Appl. Opt.* **48**(10), D163–D168 (2009).
11. I. Ferulova et al., "Photodiode based prototype device for skin autofluorescence photobleaching diagnostics in dermatology," *Lith. J. Phys.* **52**(1), 55–58 (2012).
12. A. Lihachev et al., "Photobleaching measurements of pigmented and vascular skin lesions: results of a clinical trial," *Proc. SPIE* **8087**, 80872F (2011).
13. M. P. Debreczeny et al., "Human skin auto-fluorescence decay as a function of irradiance and skin type," *Proc. SPIE* **7897**, 78971T (2011).
14. I. Ferulova, A. Lihachev, and J. Spigulis, "Photobleaching effects on in vivo skin autofluorescence lifetime," *J. Biomed. Opt.* **20**(5), 051031 (2015).
15. A. Lihachev and J. Spigulis, "Skin autofluorescence fading at 405/532 nm laser excitation," in *2006 Northern Optics*, pp. 63–65 (2006).
16. H. Zeng et al., "The dynamics of laser-induced changes in human skin autofluorescence—experimental measurements and theoretical modeling," *Photochem. Photobiol.* **68**(2), 227–236 (1998).
17. H. Zeng, "Human skin optical properties and autofluorescence decay dynamics," PhD Thesis, p. 222, University of British Columbia, Vancouver, BC (1993).
18. A. J. Berglund, "Nonexponential statistics of fluorescence photobleaching," *J. Chem. Phys.* **121**(7), 2899–2903 (2004).
19. A. Diaspro et al., "Photobleaching," in *Handbook Of Biological Confocal Microscopy*, B. J. Pawley, Ed., pp. 690–702, Springer, Boston, Massachusetts (2006).
20. L. H. Cornelissen et al., "Diffusion measurements in epidermal tissues with fluorescent recovery after photobleaching," *Skin Res. Technol.* **14**(4), 462–467 (2008).
21. L. Song et al., "Photobleaching kinetics of fluorescein in quantitative fluorescence microscopy," *Biophys. J.* **68**(6), 2588–2600 (1995).
22. N. Kollias et al., "Endogenous skin fluorescence includes bands that may serve as quantitative markers of aging and photoaging," *J. Invest. Dermatol.* **111**(5), 776–780 (1998).
23. E. Drakaki et al., "Laser-induced fluorescence and reflectance spectroscopy for the discrimination of basal cell carcinoma from the surrounding normal skin tissue," *Skin Pharmacol. Physiol.* **22**(3), 158–165 (2009).
24. B. W. Chwirot et al., "Fluorescence in situ detection of human cutaneous melanoma: study of diagnostic parameters of the method," *J. Invest. Dermatol.* **117**(6), 1449–1451 (2001).
25. M. A. Calin et al., "Optical techniques for the noninvasive diagnosis of skin cancer," *J. Cancer Res. Clin. Oncol.* **139**(7), 1083–1104 (2013).
26. R. Richards-Kortum and E. Sevick-Muraca, "Quantitative optical spectroscopy for tissue diagnosis," *Ann. Rev. Phys. Chem.* **47**, 555–606 (1996).
27. C. Choe, J. Lademann, and M. E. Darvin, "A depth-dependent profile of the lipid conformation and lateral packing order of the stratum corneum in vivo measured using Raman microscopy," *Analyst* **141**(6), 1981–1987 (2016).
28. E. G. Borisova, L. P. Angelova, and E. P. Pavlova, "Endogenous and exogenous fluorescence skin cancer diagnostics for clinical applications," *IEEE J. Sel. Top. Quantum Electron.* **20**(2), 211–222 (2014).

29. M. Skala and N. Ramanujam, "Multiphoton redox ratio imaging for metabolic monitoring in vivo," *Methods Mol. Biol.* **594**, 155–162 (2010).
30. R. Cicchi et al., "Combined fluorescence-Raman spectroscopic setup for the diagnosis of melanocytic lesions," *J. Biophotonics* **7**(1–2), 86–95 (2013).
31. Z. Huang et al., "Cutaneous melanin exhibiting fluorescence emission under near-infrared light excitation," *J. Biomed. Opt.* **11**(3), 034010 (2006).
32. D. Leupold et al., "The stepwise two-photon excited melanin fluorescence is a unique diagnostic tool for the detection of malignant transformation in melanocytes," *Pigment Cell Melanoma Res.* **24**(3), 438–445 (2011).
33. X. Han et al., "Near-infrared autofluorescence imaging of cutaneous melanins and human skin in vivo," *J. Biomed. Opt.* **14**(2), 024017 (2009).
34. I. Ferulova et al., "Influence of low power CW laser irradiation on skin hemoglobin changes," *Proc. SPIE* **8427**, 84273I (2012).
35. D. Dibbern-Brunelli, M. G. de Oliveira, and T. D. Z. Atvars, "Temperature dependence of the photobleaching process of fluorescein in poly(vinyl alcohol)," *J. Photochem. Photobiol. A* **85**(3), 285–289 (1995).
36. E. S. Wu, K. Jacobson, and D. Papahadjopoulos, "Lateral diffusion in phospholipid multibilayers measured by fluorescence recovery after photobleaching," *Biochemistry* **16**(17), 3936–3941 (1977).
37. H. Zeng et al., "Spectroscopic and microscopic characteristics of human skin autofluorescence emission," *Photochem. Photobiol.* **61**(6), 639–645 (1995).
38. J. Lesins et al., "Skin autofluorescence photo-bleaching and photo-memory," *Proc. SPIE* **8092**, 80920N (2011).
39. J. Zhao et al., "Integrated real-time Raman system for clinical in vivo skin analysis," *Skin Res. Technol.* **14**(4), 484–492 (2008).
40. J. Aziz et al., "Molecular mechanisms of stress-responsive changes in collagen and elastin networks in skin," *Skin Pharmacol. Physiol.* **29**(4), 190–203 (2016).
41. M. Foerster et al., "Confocal Raman microspectroscopy for evaluating the stratum corneum removal by 3 standard methods," *Skin Pharmacol. Physiol.* **24**(2), 103–112 (2011).
42. D. Y. Churmakov et al., "Analysis of skin tissues spatial fluorescence distribution by the Monte Carlo simulation," *J. Phys. D-Appl. Phys.* **36**(14), 1722–1728 (2003).
43. D. Falcone et al., "Microspectroscopic confocal Raman and macroscopic biophysical measurements in the in vivo assessment of the skin barrier: perspective for dermatology and cosmetic sciences," *Skin Pharmacol. Physiol.* **28**(6), 307–317 (2015).
44. A. Tfayli et al., "Discriminating nevus and melanoma on paraffin-embedded skin biopsies using FTIR microspectroscopy," *Biochim. et Biophys. Acta* **1724**(3), 262–269 (2005).
45. A. N. Bashkatov et al., "Optical properties of human skin subcutaneous and mucous tissues in the wavelength range from 400 to 2000 nm," *J. Phys. D* **38**(15), 2543–2555 (2005).
46. S. Wang et al., "Monte Carlo simulation of near infrared autofluorescence measurements of in vivo skin," *J. Photochem. Photobiol. B* **105**(3), 183–189 (2011).
47. S. Mujica Ascencio et al., "Confocal Raman microscopy and multivariate statistical analysis for determination of different penetration abilities of caffeine and propylene glycol applied simultaneously in a mixture on porcine skin ex vivo," *Eur. J. Pharm. Biopharm.* **104**, 51–58 (2016).
48. P. J. Caspers et al., "In vivo confocal Raman microspectroscopy of the skin: noninvasive determination of molecular concentration profiles," *J. Invest. Dermatol.* **116**(3), 434–442 (2001).
49. M. E. Darvin et al., "Optical methods for noninvasive determination of carotenoids in human and animal skin," *J. Biomed. Opt.* **18**(6), 061230 (2013).
50. M. Sohn, V. Korn, and G. Imanidis, "Porcine ear skin as a biological substrate for in vitro testing of sunscreen performance," *Skin Pharmacol. Physiol.* **28**(1), 31–41 (2015).
51. D. S. Mahrhauser et al., "Assessment of Raman spectroscopy as a fast and non-invasive method for total stratum corneum thickness determination of pig skin," *Int. J. Pharm.* **495**(1), 482–484 (2015).
52. M. Egawa, T. Hirao, and M. Takahashi, "In vivo estimation of stratum corneum thickness from water concentration profiles obtained with Raman spectroscopy," *Acta Dermato-Venereol.* **87**(1), 4–8 (2007).
53. M. Ashtikar et al., "Non-invasive depth profile imaging of the stratum corneum using confocal Raman microscopy: first insights into the method," *Eur. J. Pharm. Sci.* **50**(5), 601–608 (2013).
54. K. König et al., "In vivo drug screening in human skin using femtosecond laser multiphoton tomography," *Skin Pharmacol. Physiol.* **19**(2), 78–88 (2006).
55. M. E. Darvin et al., "Comparison of in vivo and ex vivo laser scanning microscopy and multiphoton tomography application for human and porcine skin imaging," *Quantum Electron.* **44**(7), 646–651 (2014).
56. E. Y. M. Bonnist et al., "Measuring the penetration of a skin sensitizer and its delivery vehicles simultaneously with confocal Raman spectroscopy," *Skin Pharmacol. Physiol.* **24**(5), 274–283 (2011).
57. C. Choe, J. Lademann, and M. E. Darvin, "Analysis of human and porcine skin in vivo/ex vivo for penetration of selected oils by confocal Raman microscopy," *Skin Pharmacol. Physiol.* **28**(6), 318–330 (2015).
58. A. Quatela et al., "In vivo Raman microspectroscopy: intra- and intersubject variability of stratum corneum spectral markers," *Skin Pharmacol. Physiol.* **29**(2), 102–109 (2016).
59. M. E. Darvin et al., "In vivo/ex vivo targeting of Langerhans cells after topical application of the immune response modifier TMX-202: confocal Raman microscopy and histology analysis," *J. Biomed. Opt.* **21**(5), 055004 (2016).
60. L. Franzen et al., "Towards drug quantification in human skin with confocal Raman microscopy," *Eur. J. Pharm. Biopharm.* **84**(2), 437–444 (2013).

Biographies for the authors are not available.